JTTEES 7:71-77

Computational Analysis of a Three-Dimensional High-Velocity Oxygen Fuel (HVOF) Thermal Spray Torch

B. Hassan, A.R. Lopez, and W.L. Oberkampf

(Submitted 11 November 1996; in revised form 14 June 1997)

An analysis of a high-velocity oxygen fuel thermal spray torch is presented using computational fluid dynamics (CFD). Three-dimensional CFD results are presented for a curved aircap used for coating interior surfaces such as engine cylinder bores. The device analyzed is similar to the Metco diamond jet rotating wire torch, but wire feed is not simulated. The feed gases are injected through an axisymmetric nozzle into the curved aircap. Argon is injected through the center of the nozzle. Premixed propylene and oxygen are introduced from an annulus in the nozzle, while cooling air is injected between the nozzle and the interior wall of the aircap. The combustion process is modeled assuming instantaneous chemistry. A standard, two-equation, k-ε turbulence model is employed for the turbulent flow field. An implicit, iterative, finite volume numerical technique is used to solve the coupled conservation of mass, momentum, and energy equations for the gas in a sequential manner. Computed flow fields inside and outside the aircap are presented and discussed.

Keywords computational fluid dynamics, gas dynamics, HVOF

1. Introduction

High-velocity oxygen fuel (HVOF) thermal spraying employs a combustion process to heat the gas flow and melt the coating material. The two-phase gas and particle flow is then accelerated to high velocities. The combustion process produces temperatures in the range of 3000 K inside the thermal spray device and high pressure sufficient enough to produce a supersonic stream exterior to the device. In contrast, plasma spray devices typically attain temperatures in the range of 10,000 K, where significant ionization of the gas mixture can occur. These high temperatures typically produce lower density, subsonic flows with lower velocities as compared to HVOF.

During the last few years, advances in computational fluid dynamics (CFD) have made their way into thermal spray modeling. Modern CFD incorporates detailed modeling of such physical phenomena as turbulence, chemical reactions, and multiphase flows to provide an in-depth understanding of the spray process and fundamentally aid in torch design. CFD simulations have been computed in two dimensions, primarily on axisymmetric thermal spray devices both with and without powder injection. The first CFD simulation of the HVOF process was conducted by Power et al. (Ref 1,2) and Smith et al. (Ref 3). They modeled the internal and external flow of the Metco diamond jet torch (Sulzer-Metco, Westbury, NY) with a powder feeder. Since the flow was choked at the exit of the nozzle, the internal flow was solved separately from the external flow. A two-step, finite-rate chemistry model was used to model the combustion of propylene (C_3H_6). For the external flow, it was assumed that all the propylene was combusted inside the nozzle and that the oxidation of carbon monoxide was small. In addition, it was assumed that the flow at the exit of the nozzle was fully mixed and had reached chemical equilibrium. Therefore, the external flow computations were performed without chemical kinetics, and only turbulent mixing with the ambient air was modeled. Particles of various sizes were injected inside the aircap and tracked subject to the local gas velocity and temperature. However, the effect of the particles on the gas stream was not modeled.

Oberkampf and Talpallikar (Ref 4, 5) also analyzed the fluid and particle dynamics of a similar axisymmetric geometry. The combustion of propylene was modeled by a one-equation, approximate equilibrium chemistry model that accounted for dissociation of the combustion products. Their work considered full coupling between the interior and exterior flow fields. In addition, the numerical algorithm used an Eulerian/Lagrangian approach for the gas and solid phases. The two phases are fully coupled through momentum and energy exchanges that appear as source terms in the governing equations. Particle temperatures and velocities that were different than the local gas flow were then allowed. Finally, characteristics such as subsonic and supersonic mixing of the various gas streams and the trajectories and phase state of the sprayed powder were investigated.

The current work presents CFD calculations made on a three-dimensional aircap similar to the Metco diamond jet rotating wire torch. A solid model representation of this aircap is shown in Fig. 1. This work concentrates on the gas dynamic aspects of these complex, three-dimensional flow fields. Features of both the interior and exterior flow fields including temperature and Mach number distributions and streamline patterns are presented and discussed.

B. Hassan, A.R. Lopez, and **W.L. Oberkampf,** Aerosciences and Compressible Fluid Mechanics Department, Sandia National Laboratories, Albuquerque, NM 87185-0825, USA.

2. Gas Dynamics Modeling

The numerical simulations are made using a commercial CFD code, CFD-ACE (Ref 6, 7). CFD-ACE is a pressure-based code that solves the three-dimensional, Favre-averaged Navier-Stokes equations that are a statement of conservation of mass, momentum, and energy for unsteady, compressible flows. The convective, or inviscid, terms are spatially differenced using either a first-order upwind scheme or a mixed second-order, central difference/upwind scheme. The second-order scheme is used with additional artificial dissipation to keep the numerical scheme stable in the presence of shock waves that exist in the solution. The diffusive terms are evaluated using a standard second-order, central difference scheme. The governing equations are solved sequentially in an implicit, iterative manner using a finite volume formulation. Each of the governing equations is solved in order with current information being used to solve the following equation at a given iteration level. This segregated solution method differs from a fully coupled solution scheme where all the governing equations are solved simultaneously at each iteration level. This scheme is an extension of the SIMPLEC method originally proposed by Van Doormaal and Raithby (Ref 8). For the present calculations, the governing equations are solved iteratively until a steady-state result is achieved. The code includes various options for modeling turbulence, reaction chemistry, and multiphase flows. For this investigation, the k-ε turbulence model of Launder and Spaulding (Ref 9) is used. Since the thermal sprayed flows of interest occur at relatively high Mach numbers where the effects of compressibility are important, the compressibility correction of Sarkar (Ref 10) is used in conjunction with the k-ε turbulence model. The reaction chemistry model is discussed in the following section. For this investigation, only single phase gas flow is simulated. Further details on the numerical algorithm and solution procedures are shown in Ref 4 to 7.

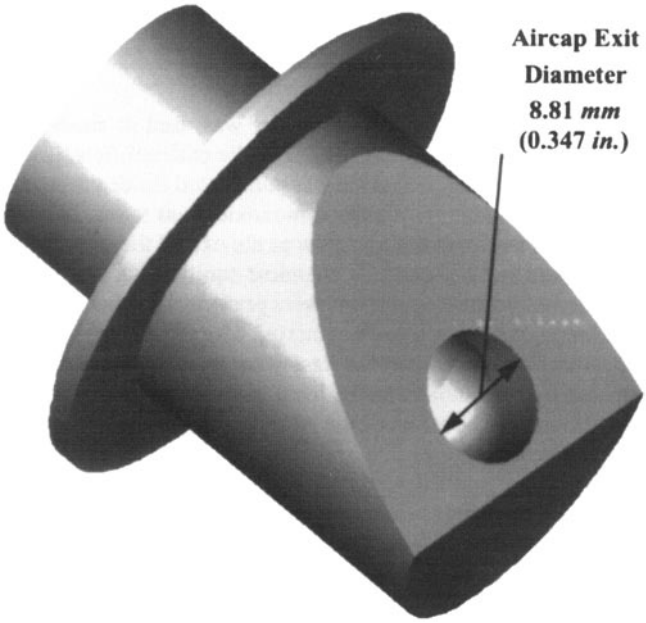

Fig. 1 Solid model of three-dimensional aircap

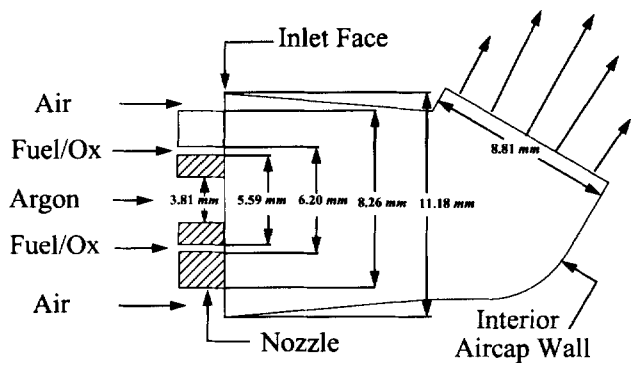

Fig. 2 Schematic of the interior of the three-dimensional HVOF thermal spray torch

3. Chemistry Modeling

Modeling of hydrocarbon chemistry can take many forms of varying complexity. The number of intermediate species and reactions that can occur in hydrocarbon-air reaction models is typically large, usually approximately 50 or more species and 100 or more reactions. Efforts at using reduced finite-rate reactions have shown mixed results, depending on how the rate coefficients are derived. Given that the time scales associated with the chemistry are much shorter than that at which the fluid convects, the assumption of equilibrium chemistry can be made. Oberkampf and Talpallikar (Ref 4, 5) reported that the typical Gibbs free energy minimization technique for computing full equilibrium chemistry can be computationally intensive and produce numerical instabilities near the inlets of the premixed streams.

The Oberkampf and Talpallikar approach made use of an approximate, instantaneous equilibrium technique. This same approach is used in the CFD calculations presented. A one-step reaction was derived from the one-dimensional equilibrium chemistry code developed by Gordon and McBride (Ref 11):

$$C_3H_6 + xO_2 \rightarrow \text{Products} \qquad \text{(Eq 1)}$$

where x is the number of moles of oxygen that react with one mole of propylene. The products of combustion in their analysis included CO_2, H_2O, CO, H_2, OH, H, and, O. Argon, the carrier gas, and nitrogen were assumed inert at the temperatures considered. A specified fuel/oxygen mixture ratio, pressure, and temperature (those of the premixed fuel and oxygen stream) are used by the one-dimensional equilibrium chemistry code (Ref 11) to determine the equilibrium composition, and from this the following balanced reaction can be determined:

$$C_3H_6 + 3.552\,O_2 \rightarrow 1.036\,CO_2 + 1.964\,CO + 1.937\,H_2O + 0.733\,OH + 0.476\,H_2 + 0.441\,H + 0.398\,O \qquad \text{(Eq 2)}$$

The above reaction will go to completion at every point in the flow field, regardless of the local temperature and pressure.

4. Aircap Geometry and Grid Generation

A schematic of the interior of the curved aircap is shown in Fig. 2. The interior of the aircap is composed of a converging conical section and two cylindrical sections blended together by a portion of a sphere. The turn angle between the centerlines of the two cylinders is 60°. There are three sets of inlet streams: the argon center stream, the premixed fuel and oxygen stream, and the air cooling stream along the surface of the aircap. In the Metco hardware, the fuel/oxygen stream is fed by 10 equally spaced holes around the circumference of the nozzle. For computational purposes, the fuel/oxygen inlet is simplified as an annulus that has the same total area as the ten holes and is centered at the same radial location as the holes in the nozzle.

The centerline of the nozzle (including the argon and fuel/oxygen inlets) has been shifted vertically upward, that is, the y-direction, by 0.406 mm (0.016 in.) from the centerline of the conical portion of the aircap. This shift provides more air cooling flow to the bottom portion of the aircap where the heat transfer rates will be higher, primarily in the curved region of the aircap near the exit. Both the premixed fuel/oxygen and the air cooling streams enter the aircap at an angle of 5°, which is the half-angle of the conical section.

The inner diameter of the aircap at the inlet face of the torch is 11.18 mm (0.44 in.), and the outer diameter of the nozzle is 8.26 mm (0.325 in.). The outer diameter of the fuel/oxygen annulus is 6.20 mm (0.244 in.), and the inner diameter is 5.59 mm (0.220 in.). The diameter of the argon inlet is 3.81 mm (0.15 in.). Finally, the aircap exit diameter is 8.81 mm (0.347 in.). All dimensions are shown in Fig. 2.

The computational grid used in the CFD calculations was created using a commercially available software package, GRIDGEN (Ref 12). The computational grid in the plane of symmetry is shown in Fig. 3, along with the exterior boundaries. The region of the grid that appears solid black is due to very dense clustering of the grid cells. The grid was created in two blocks: the interior of the aircap and the exterior where the jet decay occurs. The upper and lower exterior boundaries extend 13 aircap exit radii from the centerline, and the outlet boundary extends 20 aircap exit radii from the aircap exit. It was only necessary to solve half the three-dimensional domain due to symmetry about the x-y plane.

The computational domain in the aircap begins at the inlet where the argon, fuel/oxygen, and air streams enter the aircap. The plane of symmetry grid in the interior of the aircap is shown in Fig. 4. Radial grid clustering was performed in the regions of the shear layers surrounding the fuel/oxygen inlets and in the boundary layer on the surface of the aircap. In addition, grid cells were clustered in the jet decay region outside the torch. The grid cell dimensions in the interior are 50 (axial) × 50 (radial) × 18 (circumferential, in the half-plane). In the exterior, the grid cell dimensions are 50 (axial) × 92 (radial) × 18 (circumferential, in the half-plane) in the exterior region. The total number of grid cells in the three-dimensional calculation domain was 127,800. The results presented in Section 7 were only computed on a single grid.

Table 1 Mass flow rates and inlet temperatures

Gas	Mass flow rates kg/s	Mass flow rates scfh	Temperature, K
Argon	2.572×10^{-4}	20.0	310.0
Propylene	1.350×10^{-3}	100.0	320.0
Oxygen	4.630×10^{-3}	450.0	320.0
Air	1.024×10^{-2}	1100.0	310.0

5. Boundary Conditions

Mass flow rates and gas temperatures are specified for all three inlet streams and are listed in Table 1. All walls are modeled with a no-slip, fixed temperature condition. The wall temperature on the nozzle, that is, between the three inlet streams was 320 K. The specified wall temperature of the aircap increased linearly with x from 310 K at the inlet to 420 K at the aircap exit. The value at the exit was determined experimentally. The linear variation in temperature was judged to be more accurate than specifying a constant temperature over the entire aircap surface. For a more accurate prediction of aircap wall temperature, a coupled fluid/solid heat conduction calculation, which can be more computationally intensive, must be performed.

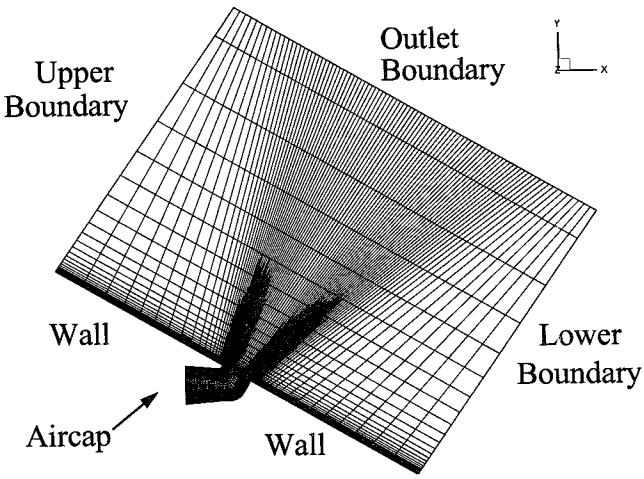

Fig. 3 Interior and exterior grid in plane of symmetry (every other grid line shown)

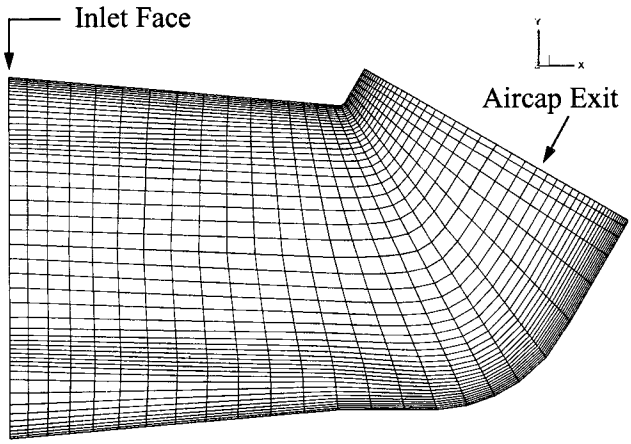

Fig. 4 Interior aircap grid in plane of symmetry (every other grid line shown)

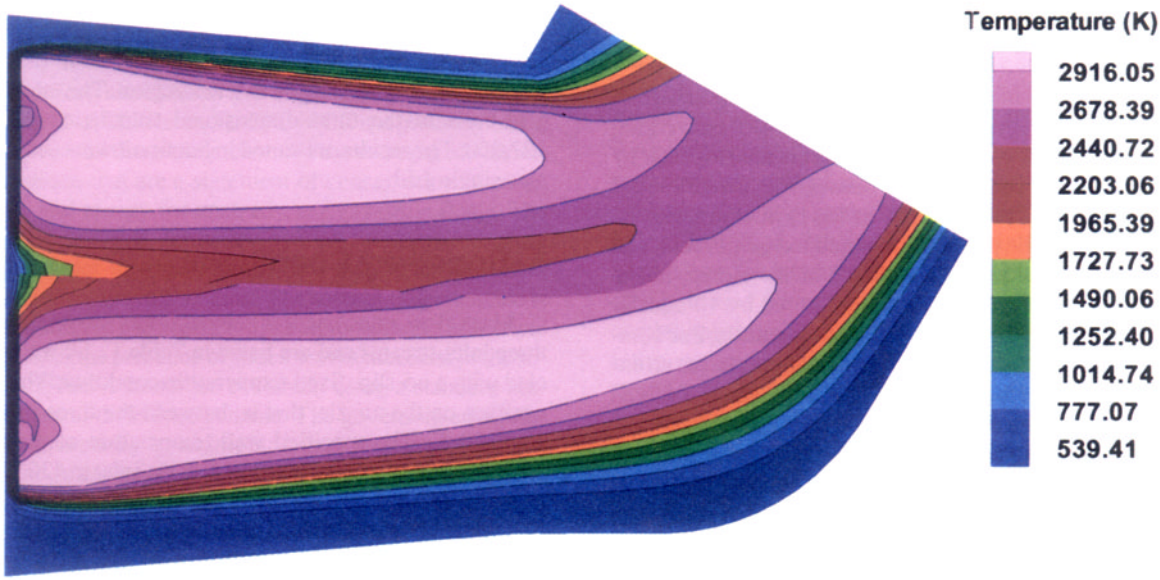

Fig. 5 Plane of symmetry gas temperature contours inside aircap

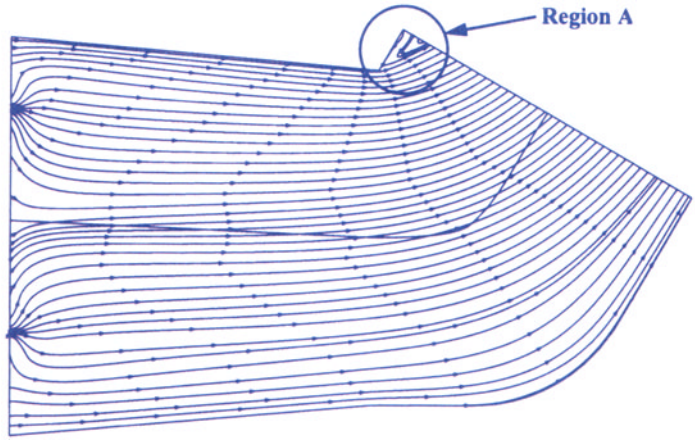

Fig. 6 Plane of symmetry streamline patterns inside aircap

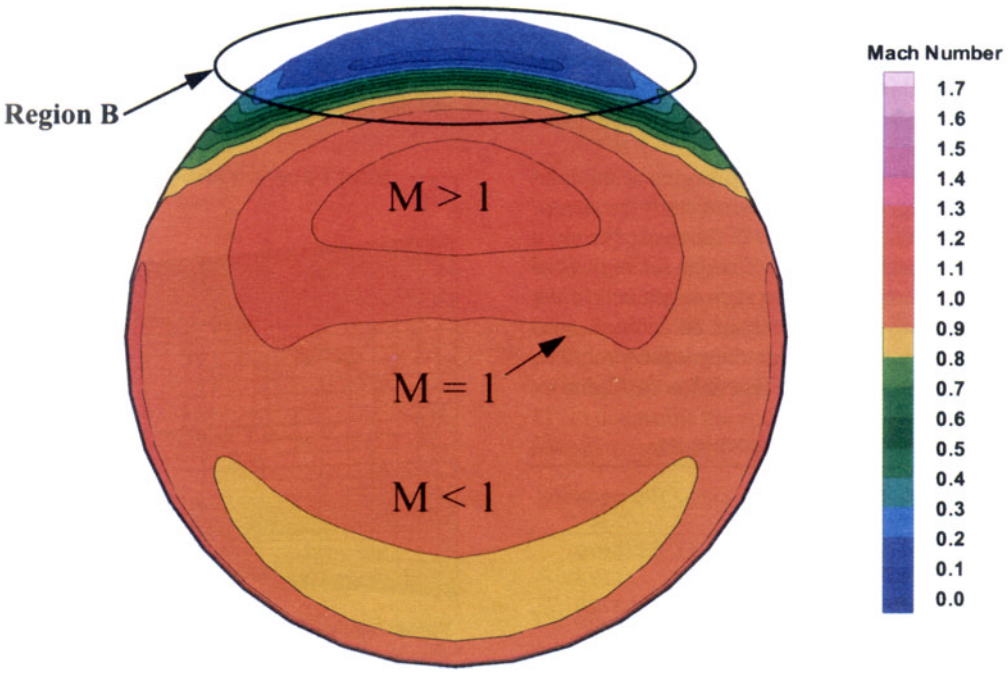

Fig. 7 Gas Mach number contours in the exit plane of the aircap

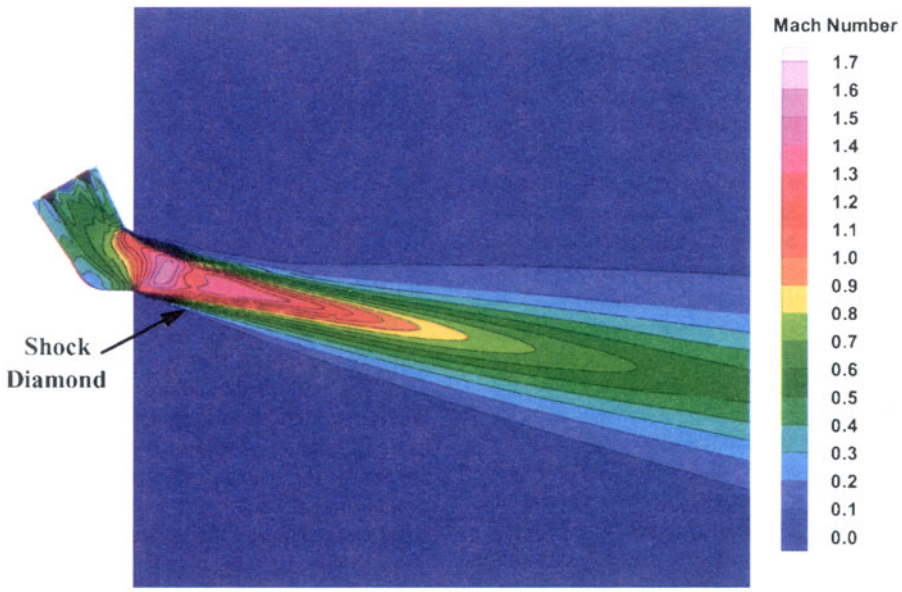

Fig. 8 Gas Mach number contours in the plane of symmetry of the aircap and exterior

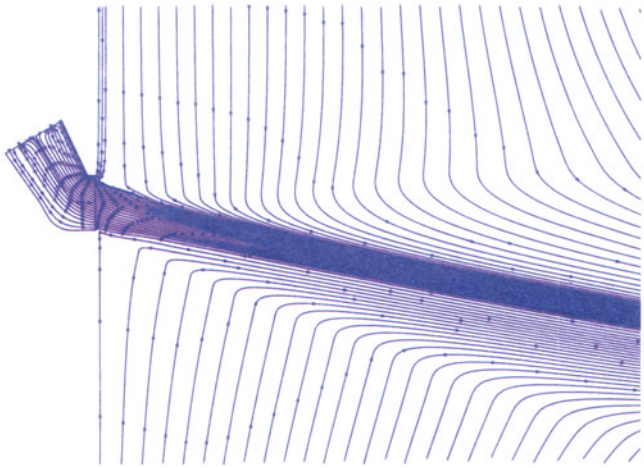

Fig. 9 Streamline patterns in the plane of symmetry of the aircap and exterior

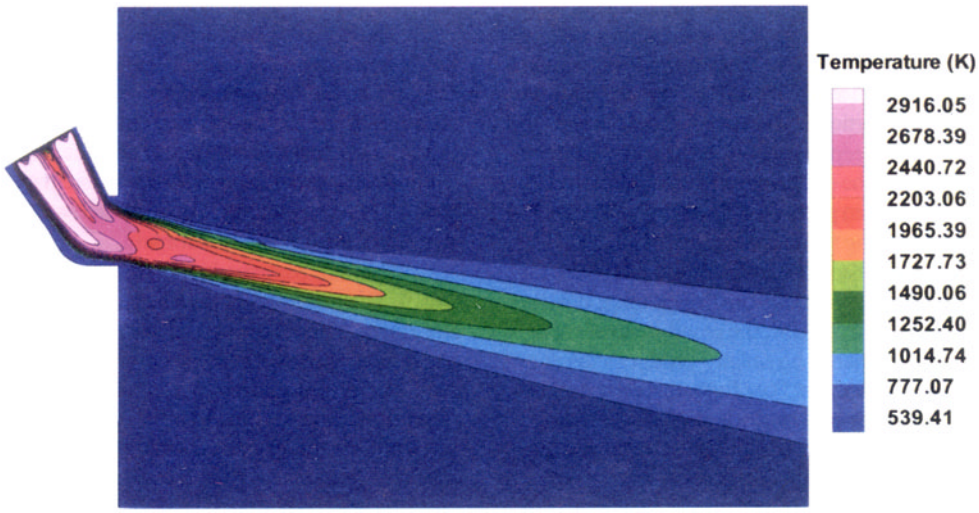

Fig. 10 Gas temperature contours in the plane of symmetry of the aircap and exterior

The HVOF torch is assumed to exhaust into ambient air at a temperature of 303 K and a sea-level pressure of 101,325 Pa (1 atm). In the exterior domain, the boundary surrounding the aircap exit, in the plane of the exit, is a fixed temperature, no-slip wall. This wall boundary assumption was made to simplify the boundary conditions and improve iterative convergence of the solution. The upper and lower exterior boundary is assumed to be fixed at the ambient pressure, but inflow and outflow are allowed. The outlet boundary, where the dominant outflow occurs, makes use of an extrapolation boundary condition. The plane of symmetry uses a symmetry condition in both the interior and exterior blocks.

6. Computational Requirements

The computational simulations were initially converged with a first-order upwind spatial discretization scheme for 1500 iterations. Since first-order upwind can be very numerically dissipative and artificially smear out high gradient regions in the flow, the solution was restarted with a mixed second-order, central difference/upwind scheme, and run for 1500 more iterations. The solution required 4.49 ms/cell/iteration of CPU time and 129 Mbytes of random access memory on a Sun Microsystems SPARCstation 10 Model 51 workstation (Sun Microsystems, Inc, Mountain View, CA). These 3000 iterations required a total CPU time of 478 h.

7. Results

7.1 *Internal Flow Field*

The gas temperature contours in the plane of symmetry of the aircap are shown in Fig. 5. The premixed fuel and oxygen enter the aircap in an annular stream and instantaneously react to form the products of combustion considered in the model. Recirculating flow regions exist on either side of the fuel/oxygen inlet and act as a flame holder. The peak temperature in the flow field is 3150 K, and this value is consistent with calculations made using the one dimensional equilibrium chemistry code of Gordon and McBride (Ref 11). The combustion region is confined on the outside by the cold air entering along the inner surface of the aircap. The air cooling is required to maintain acceptable levels of heat transfer to the aircap surface. The air cooling layer on the bottom of the aircap is thicker (as shown by the low temperature contours in Fig. 5) due to the vertical shift between the torch and the aircap, which is necessary to keep the curved portion of the aircap from melting and/or eroding. The centerline offset technique works effectively in keeping the bottom portion of the aircap cooler while minimally increasing the heating to the upper aircap wall.

Instantaneous chemistry assumes that the time scale of the reaction is much smaller in comparison to the time it takes the gas to convect downstream. In other words, the reaction rates are infinitely fast. Though instantaneous chemistry produces the correct levels of peak temperature in the flow field, it does not allow for any ignition delay. A finite-rate reaction model, alternately, would enable the gradual ignition over a finite distance and more accurately represent the combustion process. Recent work has been conducted to investigate finite-rate chemistry models for hydrocarbon combustion and has demonstrated improved results (Ref 13).

Figure 6 shows the streamline patterns in the plane of symmetry of the aircap. On the upper surface of the aircap, near the exit (as shown in region A), the boundary layer separates from the wall as the flow tries to turn the sharp corner. In this region, the streamlines show that flow from the ambient region is actually sucked into the aircap above the separated region. Near the face of the nozzle, the main ignition zone is seen by the highly curved streamlines near the fuel/oxygen inlet.

Figure 7 shows gas Mach number contours in the circular exit plane of the aircap, that is, normal to the view in previous figures. The ambient inflow region discussed in the previous figure is seen to extend over a significant portion near the top of the aircap exit (shown as region B). The sharp corner near the exit at the top of the aircap, which caused the separated shear layer, transitions into a smooth contour as one moves around the circumference toward the bottom of the aircap. One can also observe in Fig. 7 that the region below the inflow region (region B) is only partially supersonic at the exit. This means that the sonic surface is distorted in shape along the axis of the jet and lies both inside and outside the exit of the aircap. The distortion of the sonic surface near the exit occurs due to the nonuniform flow field of the mixing streams and the large variation in static temperature in the streams as shown in Fig. 5.

7.2 *External Flow Field*

Gas Mach number contours in the plane of symmetry are shown in Fig. 8. For the mass flow rates given, there is sufficient pressure from combustion to choke the flow near the exit of the aircap. In Fig. 8, the nonuniform Mach number distribution is near the exit. The peak Mach number in the supersonic jet occurs about one exit radius from the aircap and has a value of 1.7. The Mach number is the ratio of the local gas speed to the local speed of sound. Because of the high gas temperatures in the jet, the local speed of sound at the peak Mach number is about 1200 m/s.

Since the pressure exiting the aircap is higher than the ambient pressure, this under-expanded jet will then supersonically expand to the ambient pressure through a series of expansion and compression waves, known as shock diamonds. One distinct shock diamond is shown in the flow field just downstream of the nozzle exit. These expansion and shock wave patterns will be significantly more complex than typical under-expanded jets because of the highly nonuniform flow at the aircap exit. The strength of the expansion and compression waves decreases as the flow convects downstream and the supersonic core flow is dissipated due to mixing with the ambient air. The supersonic region only extends approximately halfway through the exterior portion of the calculation domain.

Streamline patterns in the plane of symmetry are shown in Fig. 9. The jet angle is not as large as the geometric turn angle of the aircap. The jet has been directed downward by the separated shear layer that exists on the upper portion of the aircap near the exit. The predicted spray angle of the torch for these operating conditions is approximately 50°, whereas the geometric turn angle is 60°. As the jet exhausts into the ambient air, a pumping effect results as the ambient air is entrained into the high speed jet. Inflow from the top and bottom boundaries occurs due to the entrainment.

The peak velocity in the jet is about 1500 m/s and decreases to a value of 300 m/s at the exit of the computational domain.

Not only does the jet velocity decrease away from the aircap, but also the gas temperature of the jet as seen in Fig. 10. The cold ambient air mixes with the hot jet and cools the flow as it convects downstream. The peak gas temperature is ~2500 K at the aircap exit. The temperature drops in the first expansion wave to ~2200 K, ~6 mm downstream of the exit. Next, the temperature rises in the first compression to ~2350 K, ~10 mm downstream. Finally, the temperature decreases to ~900 K at the exit of the computational domain. High temperature, low density jets of this type tend to decrease in temperature much faster than cold jets due to the rapid mixing that takes place with the cold ambient air.

8. Summary and Future Work

Computational solutions for a geometry similar to a Metco diamond jet rotating wire torch have been presented for both the internal combusting flow and external jet decay. Gas temperature and Mach number distributions, and streamline patterns were discussed to illustrate the features of this complex three-dimensional flow. The peak temperature in the aircap was 3150 K, and the peak Mach number in the jet, just outside of the exit, was 1.7. The predicted spray angle of the jet was seen to be ~10° less than the geometric turn angle of the aircap.

Future work will investigate coupling of spray particle dynamics and heat transfer with the gas dynamics for these three-dimensional flows. In addition, a finite-rate chemistry model will be developed and implemented to better simulate the combustion process inside the aircap. The predictions will also be compared to future experimental aircap pressure and particle velocity measurements in order to validate and build confidence in the numerical technique for computing thermal spray flows. The flow features determined through CFD calculations should be useful in the optimization of future aircap designs.

Acknowledgments

The authors wish to thank Fritz Owens and Lyle Johnson of CFD Research Corp. for their assistance throughout this investigation.

This work was performed at Sandia National Laboratories. Sandia is a multiprogram laboratory operated by Sandia Corporation, a Lockheed Martin Company, for the United States Department of Energy under contract DE-AC04-94AL85000. This work was supported under United States Department of Energy, Cooperative Research and Development Agreement No. SC92-01104.

References

1. G.D. Power, T.J. Barber, and L.M. Chiappetta, "Analysis of High Velocity Oxygen Fuel (HVOF) Thermal Torch," Paper No. 92-3598, American Institute of Aeronautics and Astronautics, July 1992
2. G.D. Power, E.B. Smith, T.J. Barber, and L.M. Chiappetta, "Analysis of a Combustion (HVOF) Spray Deposition Gun," Report 91-8, United Technologies Research Center, East Hartford, CT, March 1991
3. E.B. Smith, G.D. Power, T.J. Barber, and L.M. Chiappetta, Application of Computational Fluid Dynamics to the HVOF Thermal Spray Gun, *Thermal Spray: International Advances in Coatings Technology*, C.C. Berndt, Ed., ASM International, 1992, p 805-810
4. W.L. Oberkampf and M. Talpallikar, Analysis of a High-Velocity Oxygen-Fuel (HVOF) Thermal Spray Torch, Part 1: Numerical Formulation, *J. Thermal Spray Technol.*, Vol 5 (No. 1), 1996, p 53-61
5. W.L. Oberkampf and M. Talpallikar, Analysis of a High-Velocity Oxygen-Fuel (HVOF) Thermal Spray Torch, Part 2: Computational Results, *J. Thermal Spray Technol.*, Vol 5 (No. 1), 1996, p 62-68
6. Y.G. Lai, A.J. Przekwas, and R.M.C. So, "Aerodynamic Flow Simulation Using a Pressure-Based Method and a Two-Equation Turbulence Model," Paper No. 93-2902, American Institute of Aeronautics and Astronautics, July 1993
7. Y. Jiang, Y.G. Lai, S.Y. Ho, and A.J. Przekwas, "3D Simulations of Complex Flows with an Implicit Multi-Domain Approach," Paper No. 93-3124, American Institute of Aeronautics and Astronautics, July 1993
8. J.P. Van Doormaal and G.D. Raithby, Enhancements of the SIMPLE Method for Predicting Incompressible Fluid Flows, *Numer. Heat Transfer*, Vol 7, 1984, p 147-163
9. B.E. Launder and D.B. Spaulding, The Numerical Calculation of Turbulent Flows, *Comput. Meth. Appl. Mech. Eng.*, Vol 3, 1974, p 269-289
10. S. Sarkar, The Analysis and Modeling of Dilatational Terms in Compressible Turbulence, *J. Fluid Mech.*, Vol 227, 1991, p 473-493
11. S. Gordon and B.J. McBride, "Computer Program for Calculation of Complex Chemical Equilibrium Compositions, Rocket Performance, Incident and Reflected Shocks, and Chapman-Jouguet Detonations," SP-273, Interim Revision, NASA-Lewis Research Center, March 1976 (New Version 1989)
12. *GRIDGEN User's Manual*, Version 10, Pointwise, Inc., Bedford, TX, 1995
13. B. Hassan, W.L. Oberkampf, R.A. Neiser, A.R. Lopez, and T.J. Roemer, "Computational and Experimental Investigation of High-Velocity Oxygen-Fuel (HVOF) Thermal Spraying," Paper No. 96-1939, American Institute of Aeronautics and Astronautics, June 1996